International Journal of Heat and Technology
Vol. 44, No. 1, February, 2026, pp. 132-142
Journal homepage: http://iieta.org/journals/ijht

Prediction of Critical Heat Flux and Pool Boiling Heat Transfer Coefficient Using Artificial Neural Network

Kumar Chougala*, Sidramappa Alur

S.G.Balekundri Institute of Technology, Belagavi 590010, India

Corresponding Author Email: kumar.chougala@gmail.com

https://doi.org/10.18280/ijht.440111

Received: 25 July 2025
Revised: 19 January 2026
Accepted: 2 February 2026
Available online: 28 February 2026

Keywords:
Artificial Neural Network, predictive modeling, pool boiling heat transfer coefficient, critical heat flux

ABSTRACT

The commonly used fluids, such as normal water, distilled water, RO water, lubricating oil, and ethanol, have been boiled off over a Ni-Cr heater, and their pool boiling heat transfer characteristics have been determined experimentally. It has been found that distilled water typically exhibits a relatively higher Pool Boiling Heat Transfer Coefficient (PBHTC) and Critical Heat Flux (CHF) value, while the lowest CHF is exhibited by the lubricating oil. Ethanol, in comparison to the water-based fluids, yielded a lower CHF value but demonstrated a higher CHF value than the lubricating oil. The experimental readings have been used to develop the predictions by Artificial Neural Network modelling. It has been found that ANN models were able to predict the pool boiling heat transfer coefficients, but they underpredicted the CHF value with a maximum deviation of 5%. The Levenberg-Marquardt and Scaled Conjugate Gradient machine learning models are used in this study. Among the two models that were developed, the Levenberg-Marquardt Machine Learning method was able to predict the critical heat flux and boiling heat transfer coefficient with the Mean Squared Error (MSE) of 0.01303 and 0.06021, and coefficient of determination (R^2) of 0.9571 and 0.9996, respectively.

1. INTRODUCTION

Understanding and accurately predicting the heat transfer coefficients during pool boiling is essential for optimizing the efficiency and performance of these systems. Conventional techniques for predicting the boiling heat transfer coefficient in pool boiling frequently depend on empirical correlations obtained from experimental data. While these correlations provide valuable insights, they are typically limited in their applicability to specific fluids, heating surfaces, and operating conditions. Moreover, they may not capture the complex nonlinear relationships inherent in the boiling process, leading to inaccuracies in predictions.

Artificial Neural Networks, or ANNs, have become extremely effective tools for simulating intricate physical processes in recent years and are superior to traditional methods in a number of ways, such as their capacity to capture nonlinear relationships, adapt to a variety of datasets, and generalize effectively to previously unseen data. Furthermore, by gaining a deeper understanding of the physics behind pool boiling, the sensitivity analysis of the ANN model can further the field of heat transfer science and technology.

The purpose of this study is to investigate the use of artificial neural networks to model pool boiling heat transfer. The ANN model is trained and validated using experimental data collected under various boiling conditions, such as different fluids, heating surfaces, excess temperature, and thermal conductivity. Various network architectures and training algorithms are tested to improve the model's predictive performance. The creation of a precise ANN-based pool boiling heat transfer model will have a big impact on engineering design and optimization. By providing reliable predictions of critical heat flux and heat transfer coefficients, such a model can facilitate the development of more efficient and cost-effective thermal systems.

Kumar et al. [1] utilized 180 data sets created from the pool boiling experiments conducted over the coated copper surface to develop the ANN models for the prediction of PBHTC. Gajghate et al. [2] were able to improve the PBHTC by 50 % at 0.04% concentration of Graphene /Water-Dimethylformamide Nanofluid by using a novel V-pattern staggered heater surface, and were able to predict it with more accuracy using Random Forest Regression (RFR) as an ANN tool. Serrao et al. [3] utilized the existing database of pool boiling experiments conducted on water to develop the ANN models for predicting the Critical Heat Flux (CHF). Rashidi et al. [4] utilized the experimental readings obtained while boiling FC-72 in a horizontal channel with fins to develop the ANN model to predict the Pool Boiling Heat Transfer Coefficient (PBHTC). Fazel [5] modified an ANN model with a ReLU activation function to correct the existing correlation for estimating the bubble departure diameter, which had about 40% deviation with respect to the experimental data. Mehdi et al. [6] used about 1200 experimental data covering pool boiling of 07 fluids over twenty different types of enhanced surfaces, and they developed a deep neural network-based model that was able to predict the PBHTC with improved accuracy.

Rashidi et al. [7], after reviewing the research works on pool boiling, found that artificial intelligence methods can provide more accurate predictions with R^2 values as high as 0.99, and their applications can be extended to nanofluids. Hamzekhani et al. [8] made an attempt to predict the bubble departure frequency using an ANN tool and Response Surface Methodology (RSM) of some vaporizing liquids and found that RSM outperformed the ANN in the prediction. Zhang et al. [9] found that ε-support vector machine (ε-SVM) was able to analyze the effect of heater surface material, heater surface dimensions, pressure, and orientation on the pool boiling performance over the downward-facing surfaces and predicted the CHF value more accurately than the other machine learning methods that were used. Rokoni et al [10] attempted to obtain physical descriptors of the boiling process from the experimental images and matched them with the number and diameter of bubbles obtained by a deep learning algorithm over multiple datasets and heater surfaces. Scariot et al. [11] used video frames obtained during the boiling of water over a horizontal heater to train the deep convolutional neural network (CNN). McClure and Carey [12] tried to get new insights into the interaction of gravity and Marangoni effects during the boiling process by using a genetic algorithm and deep learning. Calati et al. [13] investigated the role of aluminum metal foams in the enhancement of the heat transfer performance under pool boiling conditions. They developed an ANN model to predict the heat transfer coefficient within 10% of the measured data. Sajjad et al. [14] used a deep learning method to predict the heat transfer over the heated surfaces having different roughness values. An optimal model was developed using a huge amount of data and was able to estimate the PBHTC with a coefficient of determination (R^2) = 0.994. Peng et al. [15] used the laboratory data of Fe_3O_4/water nanofluid pool boiling for training the network and studied the effect of concentration, heat flux, and roughness on PBHTC and superheat temperatures. Rassoulinejad-Mousavi et al. [16] used deep learning (DL) models obtained from the images captured while conducting the experiments to detect the CHF. CNN and transfer learning (TL) were used, and TL was found to outperform CNN in the prediction. Sajjad et al. [17] used an AI-based method that considered the porosity and coating thickness of the sintered coated and porous coating and were able to predict the PBHTC with an overall R^2 = 0.976 with an optimized deep neural network model. Pare and Ghosh [18] conducted the surface examination of the alumina-based nanofluids post the boiling experiments by measuring surface roughness and the microscopic images. They also conducted the ANN model analysis, and the best model was selected based on the number of training cycles required and the MSE (Mean Squared Error). Swain et al. [19] used isopropyl alcohol as the solvent fluid and ammonia chloride as the surfactant and obtained an improvement in the value of PBHTC with 200 PPM of surfactant. They used RBN and found it to be more accurate in comparison to the existing correlations. Gajghate et al. [20] conducted a pool boiling experiment of deionized water by varying the thickness of the graphene coating over the copper surface and were able to predict the PBHTC using a MATLAB-based ANN model.

McClure and Carey [21], while exploring the dependency of heat flux on various parameters during nucleate boiling using Machine Learning as a tool, brought new insights into the interaction of gravity and Marangoni effects during the boiling process. Zarei et al. [22] relied on the existing experimental data to develop the ANN model for the prediction of PBHTC of refrigerant-based nanofluids and were able to predict the PBHTC more accurately with the correlation coefficient (R^2) of 0.9948 with the developed LM model. Alavi Fazel and Lorzadeh [23] introduce a novel method of accelerating the pool boiling heat transfer process by making the electrolysis and boiling processes occur simultaneously. The heating surface is stimulated by DC electricity, and the extra bubbles are generated, resulting in a turbulated nucleation phase. They also analysed the experimental data with an ANN model. Ravichandran and Bucci [24] presented a fast, online method for the measurement of pool boiling parameters based on the radiation recorded by a high-speed camera. Mansour et al. [25] used a fuzzy logic-based method for predicting the PBHTC of refrigerant R-134a and used the Mamdani method for the modelling. The proposed Fuzzy logic method showed a maximum deviation of ± 6% with the experimental results. Qiu et al. [26] developed an ANN model adopting a comprehensive physics and data-driven approach for the prediction of flow boiling heat transfer rate in mini/micro channels. A huge database was used, and the ANN was thoroughly optimized for its input parameters. He and Lee [27] investigated the effect of the material of the heater and size on the CHF and found fluid properties were the most influential parameters as compared to heater surface morphology. Aliç et al. [28] recognized 18 different parameters from the available correlations for estimating the pool boiling heat flux and considered 06 mechanisms of the heat flux equations in the isolated bubble regime. They used Genetic algorithms, ABC algorithms, SVM, DT, and MLP, and the SVMReg method was found to be more accurate compared to the other correlations. Gajghate et al. [29] were able to improve the pool boiling heat transfer performance up to 2600 ppm of ammonium chloride.

Gajghate et al. [30] used the dip nanocoating method to deposit coatings over the copper heater and investigated the effect of coating thickness on PBHTC of deionized water by both experimental and numerical methods. The augmentation in PBHTC value obtained was 53% for the surface roughness value of 124%, and was verified by both methods.

ANN models developed so far for the prediction of heat transfer coefficients are based on the experimental data base that was available in the literature and taken from different environments of experimental conditions involving several parameters, and have not been consistent because of the combined effect of several parameters. One may not be able to understand the direct influence and contribution of each of the parameters in the improvement of PBHTC and CHF value. We have used the commonly used fluids such as normal water, osmosis water, distilled water, and lubricating oil, etc., which would contribute to a range of Nanofluids for various industrial and medical applications. The ANN model developed in the present work has been created from the limited and yet reliable experimental data. An ANN model has been developed by standardizing the inputs and choosing the best ANN architecture and training techniques to reduce overfitting, and it should be helpful for developing ANN models in the future while handling nonlinear data.

2. BASE FLUIDS PREPARATION

The base fluids used in this research paper are normal water,

osmosis water, distilled water, and lubricating oil, which have been taken from our college's chemistry and energy conversion laboratories, respectively. The 100 ml of ethanol has been purchased from Dodhaganga Krishna Sahakari Sakkare Karkhane Niyamit Chikodi. The five base fluids of each 100 ml have been stored in the bottles. The prepared base fluids have been tested for thermal conductivity, viscosity, and surface tension.

3. POOL BOILING EXPERIMENTAL SETUP

The components of the pool boiling heat transfer apparatus, as shown in Figure 1, consist of the boiling chamber with glass for the visualization, the heater element, the power source with dimmerstat, cooling water arrangement with pump, instrument box with a slot for SD card and the electric power control system This new equipment uses electrically heated resistor wire as the heat source. Water purified by the reverse osmosis process or distilled water is used as the fluid. A suitable length of the resistance wire is taken, and its ends are bent and fixed to the silver-coated copper lugs as shown in Figure 2. The effective length of the wire between the lugs was measured accurately. The connecting flat surfaces from both the leads and the copper shoes were polished regularly to ensure proper electrical contact. The lugs at the end of the resistor wire are then fixed securely to the leads by screws. Nearly 4 litres of distilled water were taken in the beaker. The copper leads and the immersion coils are assembled as shown in Figure 1. The polarity of the power source and the thermocouples or temperature sensor must be maintained as indicated. Additional illumination may be provided for making a good-quality video during measurements to capture the boiling phenomena. The temperature controller is set to the desired level. Voltage is increased continuously and slowly. The rate of increase of the voltage depends on the laboratory conditions. It is suggested that the total time for burnout or maximum current/voltage (limited by the power source) may be achieved in about 10 minutes.

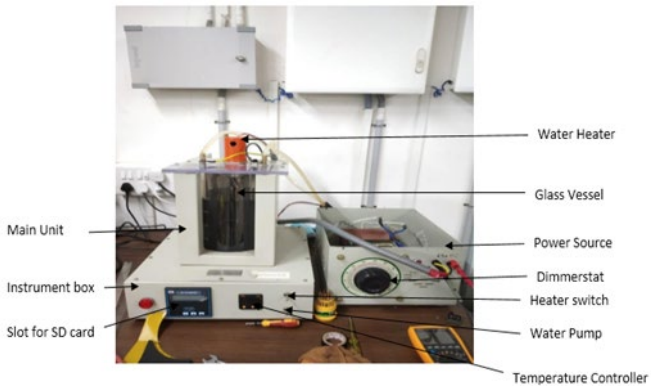

Figure 1. Pool boiling experimental setup

The test wire of 0.54 mm diameter and 135 mm length made of Ni-Cr (80:20) was connected to the heater terminals. The test wire was connected to the heater terminals and was placed in the container containing distilled water. The main heater was switched on, and water was heated to the desired temperature of 60 °C. The test heater wire was then heated by switching on the test heater wire. The power given to the test heater wire is adjusted and increased in steps by using the dimmerstat. Note the voltage, current, water bath temperature, and surface temperature of the test wire. Repeat the experiment with different reverse osmosis water. Repeat the procedure for the remaining base fluids (Figure 3). The heat flux and pool boiling heat transfer coefficients were then calculated. Plots of heat flux versus excess temperature and boiling heat transfer coefficient versus heat flux were plotted.

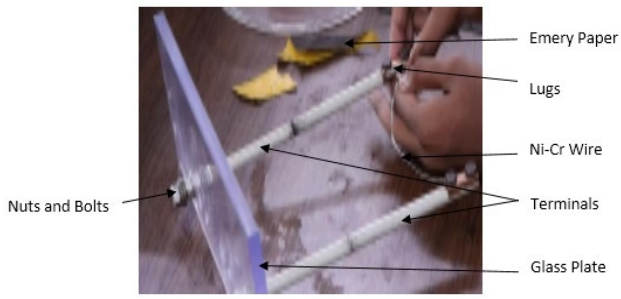

Figure 2. Preparation and fixing of the Ni-Cr circular heater on the copper electrodes

Figure 3. Base fluid samples

4. POOL BOILING HEAT TRANSFER CALCULATION

Heat Transfer rate (Q): $Heat$ Transfer rate $= voltage \times current$.

$$Q = V \times I \text{ in Watt} \quad (1)$$

Heat Flux (q): $Heat\ flux = \frac{heat\ transfer\ rate}{area}$.

$$q = \frac{Q}{A} \quad \text{in} \frac{W}{m^2} \quad (2)$$

Area of experimental wire (A): $Area = \pi \times Length\ of\ test\ wire \times Diameterof\ test\ wire$.

$$A = \pi \times L \times D \quad in\ m^2 \quad (3)$$

Boiling Heat transfer coefficient (h): $Boiling\ Heat\ transfer\ coeffiecient = \frac{heat\ flux}{excess\ temperature}$.

$$h = \frac{q}{\Delta T} \quad in W/m^{2\cdot}{}^{\circ}C \quad (4)$$

5. RESULTS AND DISCUSSIONS

Figure 4 depicts that water-based fluids exhibited higher

CHF values compared to lubricating oil and ethanol due to the favorable thermophysical properties in the thermal conductivity and viscosity values. Lubricating oil showed the lowest CHF among the tested fluids, likely due to its higher viscosity and lower thermal conductivity, which delays the growth of bubbles and the heat transfer rates achievable. Ethanol, in comparison to the water-based fluids, yielded a lower CHF value but demonstrated a higher CHF value than the lubricating oil, possibly due to its lower surface tension.

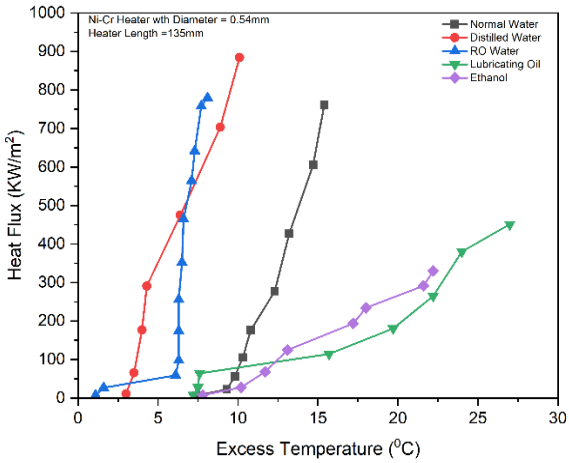

Figure 4. Pool boiling curves for different base fluids

5.1 Effect of heat flux on boiling heat transfer coefficient

Figure 5 depicts the heat flux and PBHTC values measured for distilled water, reverse osmosis water, lubricating oil, and ethanol. The impact of distilled water, RO water, lubricating oil, and ethanol on CHF and PBHTC in pool boiling applications varies depending on their thermal characteristics, surface tension, viscosity, and other parameters. It is understood from Figure 5 that the distilled water typically exhibits relatively higher PBHTC and CHF values due to its low surface tension, high thermal conductivity, and favourable wetting behaviour. Efficient nucleate boiling and rapid bubble detachment contribute to high CHF, while strong liquid-solid contact enhances PBHTC.

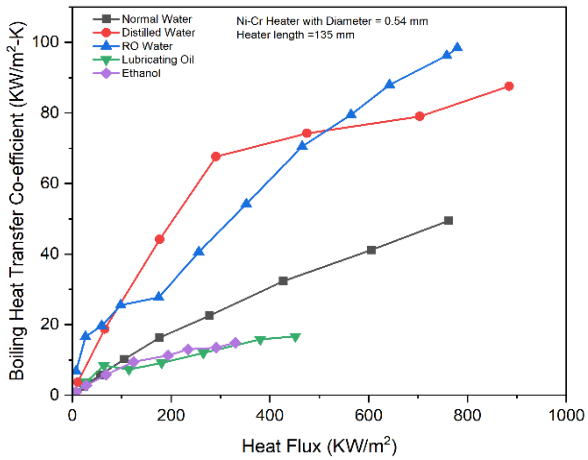

Figure 5. Effect of heat flux on PBHTC of base fluids

The lower boiling point of distilled water allows for rapid vapor bubble formation and growth, leading to improved heat transfer rates.RO water shares similarities with distilled water in terms of thermal properties but may contain fewer dissolved impurities. Similar to distilled water, RO water is expected to exhibit relatively high CHF and PBHTC, although potential differences in fluid purity may lead to slight variations in boiling behaviour. Lubricating oil generally has low thermal conductivity and higher viscosity compared to water-based fluids. These properties may result in lower critical heat flux and heat transfer coefficient due to slower heat transfer rates and hindered bubble dynamics. The higher boiling point of lubricating oils may also contribute to reduced CHF compared to water-based fluids. Table 1 depicts the comparison of CHF and BHTC experimental values of base fluids and ANN at the burnt-out point.

Table 1. Comparison of CHF and BHTC experimental values of base fluids with ANN at the burnout point

Base Fluids	Experimental CHF (KW/m^2)	Artificial Neural Network Model (KW/m^2)	Experimental BHTC ($KW/m^2{\cdot}°C$)	Artificial Neural Network Model ($KW/m^2{\cdot}°C$)
Normal water	761.57	728.89	49.5	49.47
Distilled water	884.54	846.59	87.58	87.53
RO water	779.48	746.04	96.23	96.18
Lubricating oil	451.35	431.98	16.72	16.71
Ethanol	330.13	315.96	14.87	14.86

6. NUMERICAL METHODS

6.1 Artificial Neural Network approach

A dependable database is necessary for training, testing, and validating artificial neural networks. The pool boiling heat transfer experimental results for five base fluids were chosen to train the ANN model. To create an ANN model, the available experimental data is divided into three sets: training, testing, and validation sets.

In this paper, to train an artificial neural network, 84 pool boiling experimental data with five base fluids over a Nickel-Chromium heater surface are used. The neural network develops a prediction accuracy by correlating the input and output parameters. Thermal conductivity, viscosity, surface tension, excess temperature, surface temperature, and heat flux are the input parameters for the Artificial Neural Network, whereas the output parameters chosen are the Critical Heat Flux and Boiling Heat Transfer Coefficient.

6.2 Neural network architecture

Multilayer neural networks have been used in network architecture for learning purposes because of their ability to learn nonlinear and complex decision-making problems. The feed-forward back-propagation algorithm is the most frequent

method for training multilayer neural networks. The neural network structure consists of three layers: the input and the output separated by a series of hidden layers, as shown in Figure 6(a) and (b). Inputs are given at the input layer, and the hidden layers are the ones where the deep learning and computational work is done. One neuron has been allotted for each of the inputs so that the number of neurons is equal to the number of input variables. The third layer of a neural network is where we will get the predicted output value. The feed-forward network architecture is considered, where the information passes straight from the left to right with as many hidden layers as required without the information being looped around, and the network's transfer function in the hidden layer is sigmoid. Because of its derivability, this form of transfer function is one of the most essential, and it is classified into two types: single-pole (logsig) and bipolar (tansig) sigmoid.

6.3 ANN performance evaluation

In this study, performance metrics such as MSE and R^2 were used to evaluate the effectiveness of the artificial neural network, the Eqs. (1) and (2) represent the expression for computing the MSE and R^2 [4, 5], where n, $q_{exp,}$ and $q_{prd.}$ represent the number of experimental data samples and predicted outcomes by the applied models. The difference between those two should be minimized to achieve excellent performance.

$$MSE = \sum \frac{1}{n} \sum_{k=1}^{n} \left(q_{exp} - q_{pre}\right)^2 \tag{5}$$

The R^2 is used to compare the outputs with targets and indicates the strength of the relationship between the targets and outputs. The range of R^2 is between -1 and 1. When the value of R^2 is positive, there is a solid interrelation among the data. On the contrary, a negative 1 indicates a solid negative interrelation, and 0 means no connection between these two variables.

$$R^2 = \frac{\Sigma\left[\left(q_{exp} - z_{exp}\right) * \left(q_{pre} - z_{pre}\right)\right]}{z_{exp} * z_{pre}} \tag{6}$$

where, z_{exp} and z_{pre} are the mean values of q_{exp} and q_{pre} similarly z_{exp} and z_{pre} are considered deviations of q_{exp} and q_{pre}. respectively. The results indicated in Tables 2 and 3 show that the lowest values of MSE and higher values of R^2 are considered optimum outcomes, and these were obtained with ten neurons in the hidden layer.

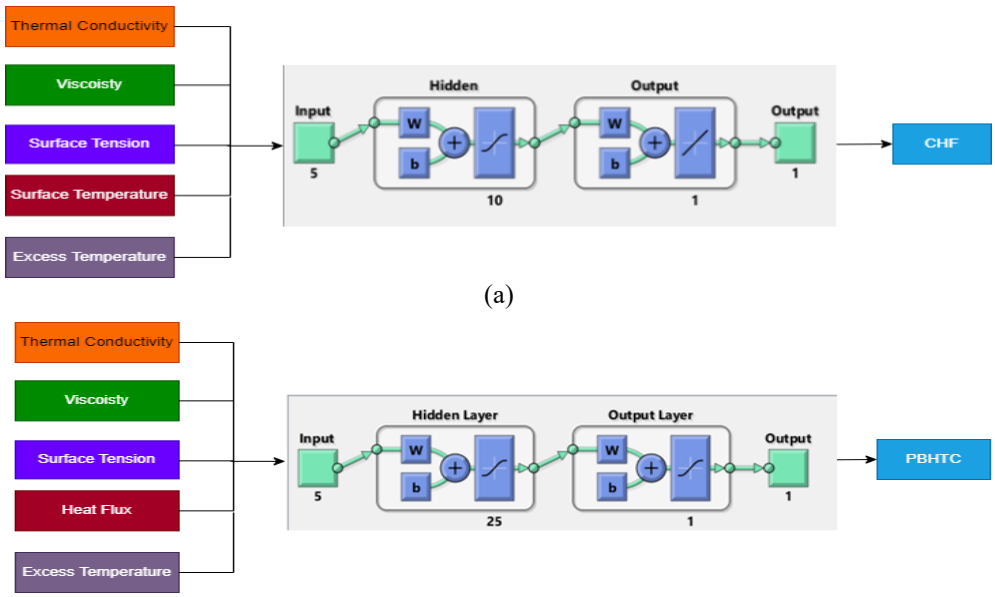

Figure 6. CHF and BHTC network architectures for 10 and 25 neurons

Table 2. Optimal parameters for CHF and BHTC with the LM machine learning model

Base Fluids Predicted Data	Machine Learning Algorithm	Activation Function	Optimal Number of Neurons	Database	MSE	R^2
Heat Flux	Levenberg-Marquardt	TANSIG	10	Train Test Validation	0.04442 0.08466 0.01303	0.4637 0.5054 0.9571

Table 3. Optimal parameters for BHTC with the Levenberg-Marquardt machine learning model

Base Fluids Predicted Data	Machine Learning Algorithm	Activation Function	Optimal Number of Neurons	Database	MSE	R^2
Boiling Heat Transfer Coefficient	Levenberg-Marquardt	TANSIG	25	Train Test Validation	5.353 2.56 0.06052	0.9995 0.9986 0.9996

6.4 Best validation performance

Figures 7 and 8 show the best validation performance as measured by the mean square error and number of sample repetitions. The validation process will continue until the error value is as low as feasible. The validation data shows the best validation performance, with the outputs of the critical heat flux and the boiling heat transfer coefficient attaining error values of 0.03558 and 4.906 after 18 and 5 optimal neurons. Nonetheless, the CHF and PBHTC for the test data have mean square errors (MSEs) of 0.3142 and 0.3985, respectively.

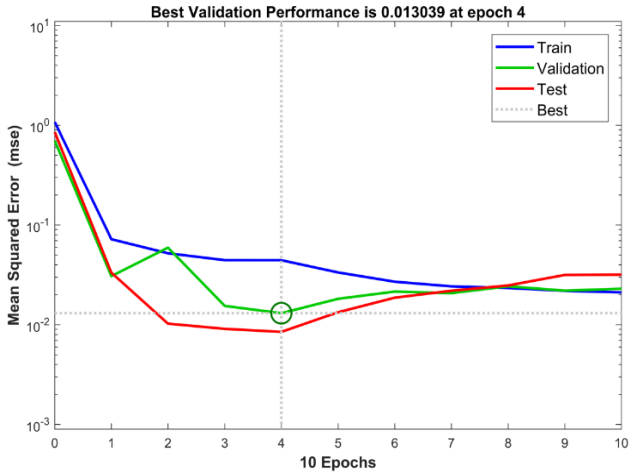

Figure 7. CHF best validation performance graph

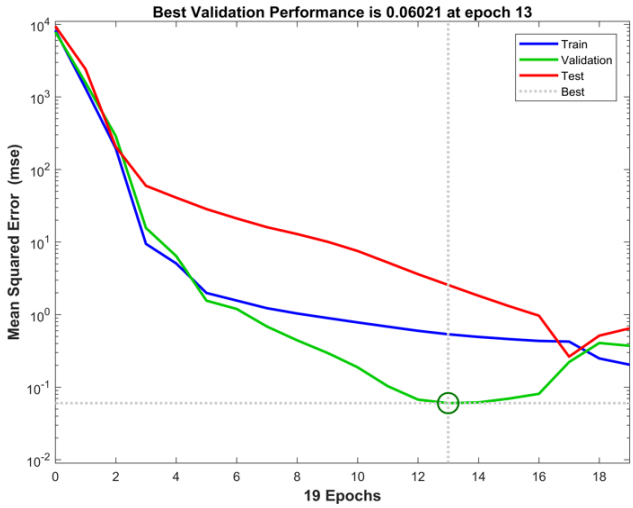

Figure 8. BHTC best validation performance graph

6.5 Regression graphs

Figures 9 and 10 depict the regression graphs used to show how the output deviates from the target. The regression graph's horizontal and vertical axes indicate the neural network's output and target values, respectively. This curve has three regression graphs, one each for the test, training, and validation data. The network was trained using 70% of the data, then tested with 15% of the data. The remaining 15% of data is used for network validation. Key parameters that are in optimal condition in each of the three graphs include regression value, slope, and y-intercept. A dashed line shows that the output and target are in perfect match. When the regression and slope are closer to unity, and the y-intercept value is closer to zero, the correlation between the output and the target improves. values of 0.03558 and 4.906 after 18 and 5 optimal neurons. Nonetheless, the CHF and PBHTC for the test data have MSEs of 0.3142 and 0.3985, respectively.

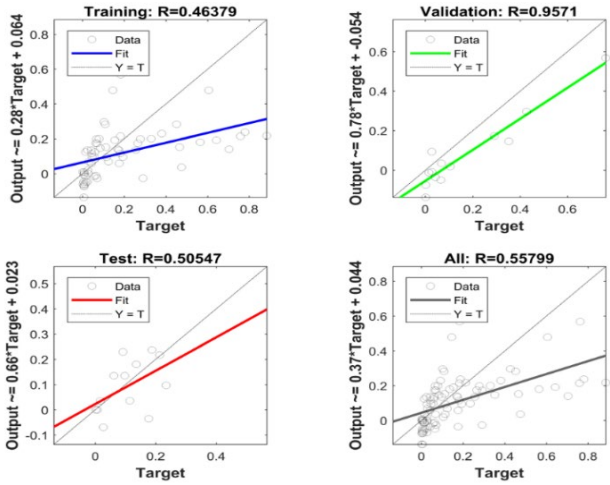

Figure 9. CHF regression graph

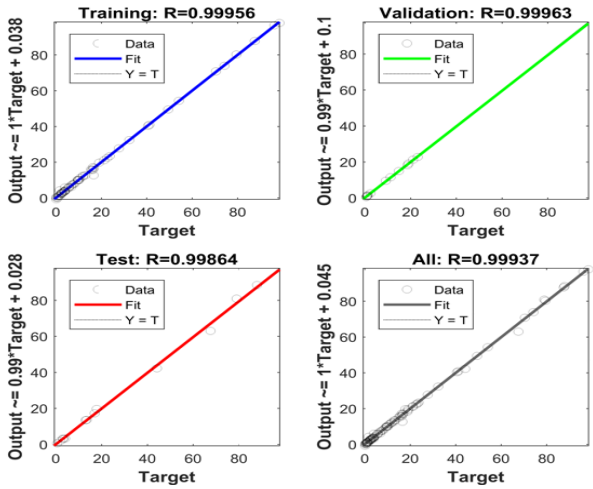

Figure 10. BHTC regression graph

6.6 Histogram error graphs

Figures 11 and 12 show the histogram error for the problem outputs, with the error value and frequency displayed on the horizontal and vertical axes, respectively. To meet the model's requirements, including minimum tolerance, the model, which is predicted by the network using the input and target data it provides, as well as the training algorithm chosen, will modify weights and biases using training rules. Tolerance is calculated by subtracting the network output values from the target data. When the output value exceeds the target value, a minus sign shows on the histogram error chart. These charts show that the training data error is close to zero. If the bars near the zero-error line lengthen, it indicates that the network was properly trained and that the model it predicted was correct.

6.7 Finding the best model

Tables 2 and 3 present the optimal parameters used for achieving the prediction accuracy as given in terms of MSE and $R^{2,}$ and thus can be used to compare and determine the best model. It can be concluded from the tables that the Levenberg-Marquardt machine learning model gave a better prediction

accuracy compared with the Scaled Conjugate Gradient model and can be used to predict the critical heat flux and boiling heat transfer coefficient for the five base fluids considered.

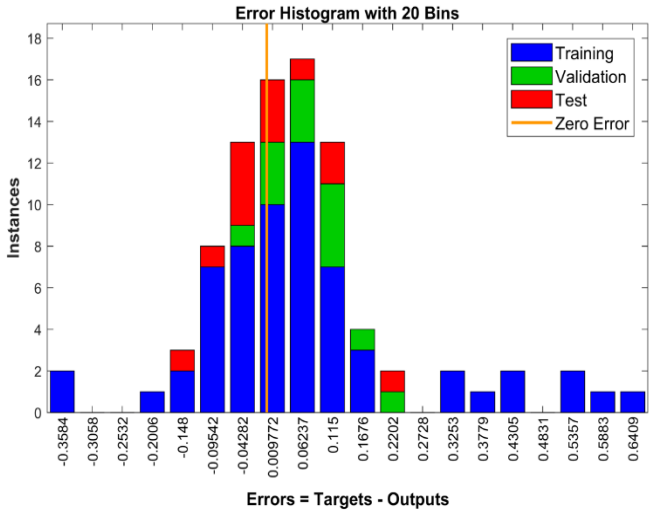

Figure 11. BHTC histogram error graph

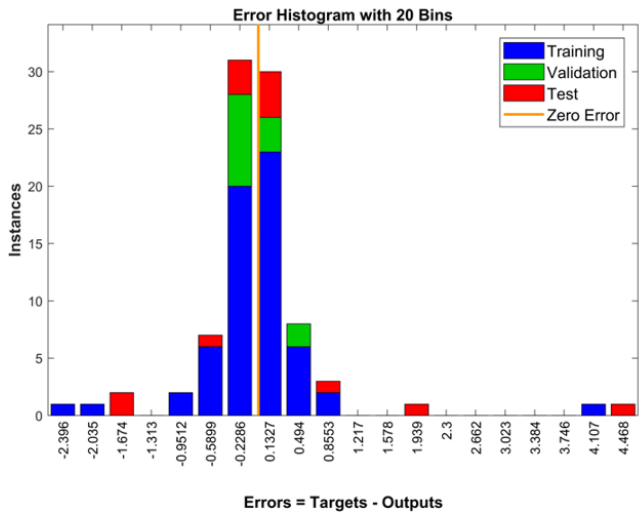

Figure 12. CHF histogram error graph

7. COMPARISON OF EXPERIMENTAL CRITICAL HEAT FLUX DATA WITH ANN MODEL

Figure 13 depicts the comparison graphs of pool boiling curves for five base fluids. A multi-layer perceptron ANN is used for the prediction of heat flux and BHTC. The backpropagation rule was used as the training algorithm. 70% of the experimental data were used for ANN training, and 15% of the data were used for testing and validation, respectively. From the figures (a to e), it was found that there is good agreement between the experimental and predicted values from the ANN. The pool boiling curves of experimental results are closer to the ANN predicted values. Therefore, the pool boiling curves drawn from experimental values with ANN are looking similar. The experimental and predicted heat flux values from ANN for normal water, distilled water, RO water, lubricating oil, and ethanol are 761.57, 884.54, 779.48, 451.35, 330.13 KW/m^{2,} and 748.16, 868.97, 765.76, 443.40, 324.31 KW/m^{2,} respectively.

7.1 Comparison of experimental boiling heat transfer coefficient data with ANN model

Figure 14 depicts the comparison graphs of heat flux v/s boiling heat transfer coefficient for five different base fluids. 70% of the experimental data were used for ANN training, and 15% of the data were used for testing and validation, respectively. From the above graphs, it was found that there is good agreement between the experimental and predicted BHTC from the ANN model. The experimental BHTC results are closer to the ANN predicted values. Therefore, the BHTC drawn from the experiments with ANN are looking similar in the graphs. The experimental and ANN predicted BHTC values for normal water, distilled water, RO water, lubricating oil, and ethanol are 49.5, 87.58, 96.23, 16.72, 14.87 KW/m^{2,}°C and 49.47, 87.53, 96.18, 16.71, 14.86 KW/m^{2,}°C, respectively.

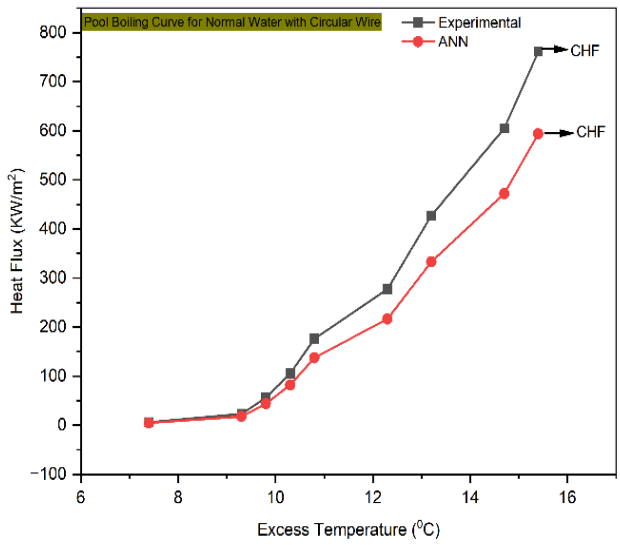

(a)

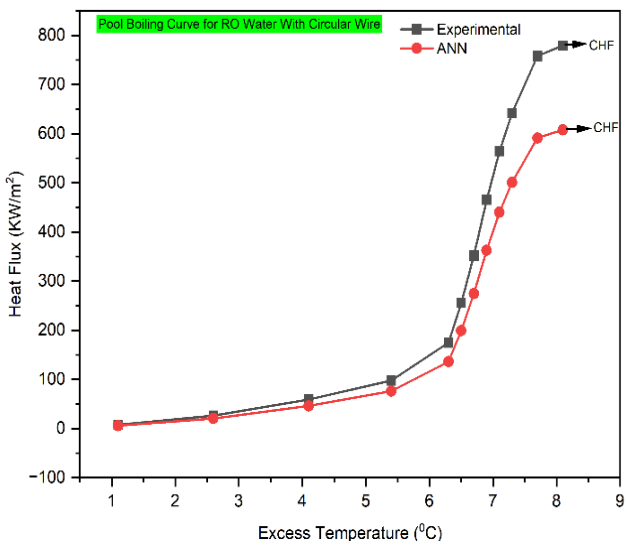

(b)

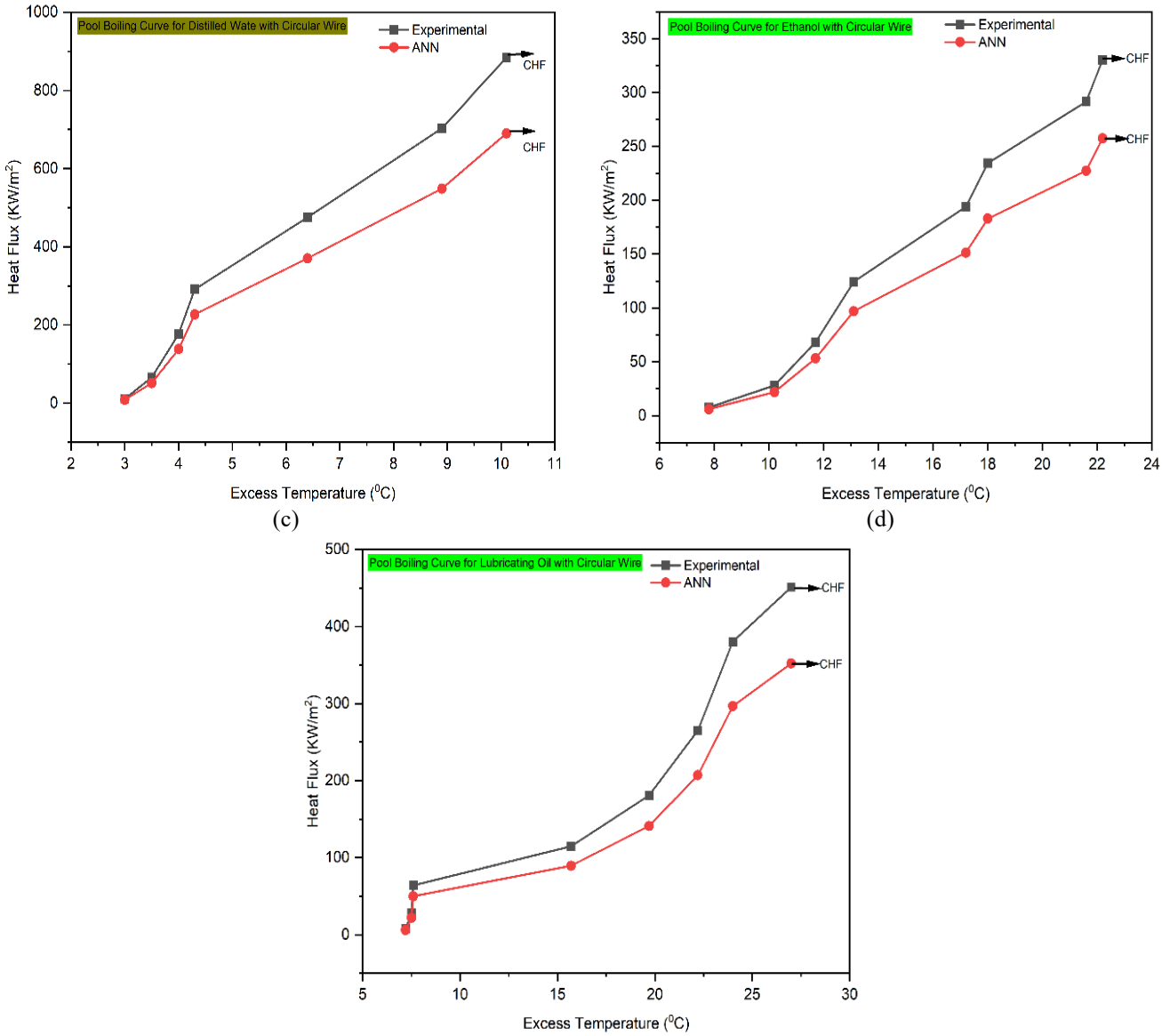

Figure 13. Comparison of pool boiling curves for various base fluids with experimental and ANN values

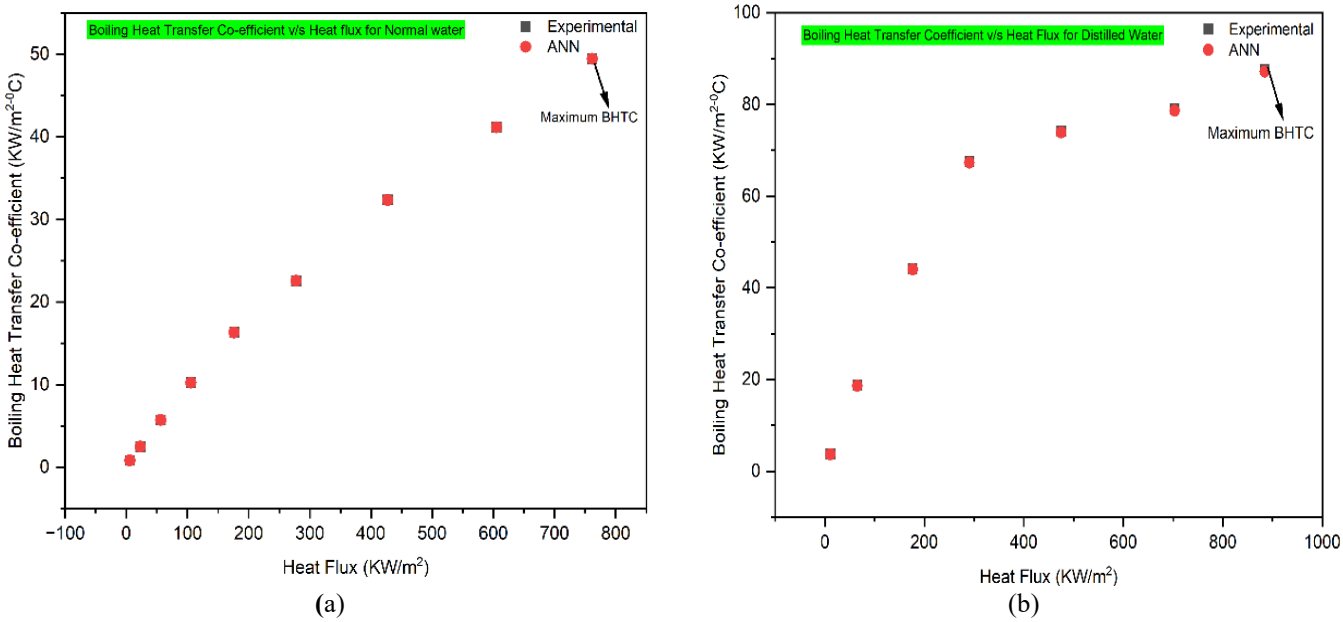

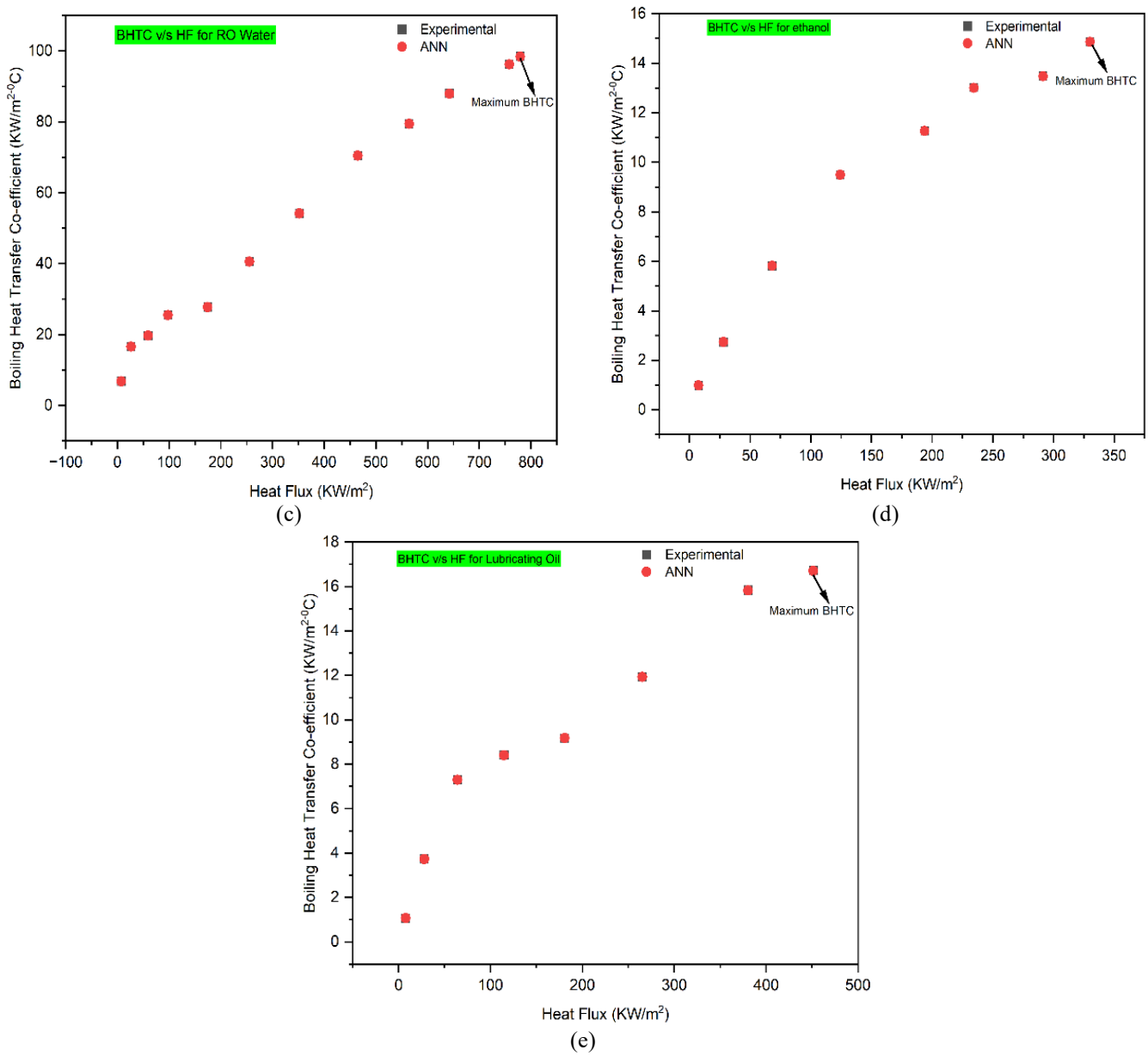

Figure 14. Comparison of heat flux v/s boiling heat transfer coefficient of experimental with ANN for five different base fluids

8. CONCLUSION

The study demonstrates the potential of ANN-based modelling as a useful tool for the design and enhancement of thermal systems in a number of industrial applications, as well as extending our understanding of pool boiling heat transfer. ANN models developed so far for the prediction of heat transfer coefficients are based on the experimental data base that was available in the literature and taken from different environments of experimental conditions involving several parameters, and have not been consistent because of the combined effect of several parameters. The ANN model developed in the present work has been created from the limited and yet reliable experimental data. An ANN model has been developed by standardizing the inputs and choosing the best ANN architecture and training techniques to reduce overfitting, and it should be helpful for developing ANN models in the future while handling nonlinear data. The solvent fluids can form a range of Nano fluids for various applications. The experiments can be extended to other solvent fluids such as Propylene Glycol, FC-72 (Perfluorohexane), refrigerants, etc. The Levenberg-Marquardt machine learning model gave a better prediction accuracy compared with the Scaled Conjugate Gradient model and can be used to predict the CHF and PBHTC for the five base fluids considered. The coefficient of determination (R^2) for CHF and PBHTC was 0.9571 and 0.9996, respectively. For distilled water, the PBHTC and CHF were optimized at 87.53 KW/m^2·°C and 846.59 KW/m^2.

9. FUTURE WORK

The dataset constraint can be addressed in future studies by increasing the number of experimental points and encompassing a larger variety of operating conditions, including different heat flux levels, wider temperature ranges, and higher nanoparticle concentrations. The ANN's capacity to generalize will be improved by adding more fluid types than the five experimented with in this work, which will enable the

model to represent a wider range of thermophysical behaviors. Comparing the performance of the ANN with that of other machine learning techniques, such as Random Forests, Support Vector Regression (SVR), Gradient Boosting, or Deep Learning models, is another intriguing avenue. The relative advantages and disadvantages of various methods for predicting nanofluid heat transfer would be clarified by such comparisons. Accuracy and interpretability may also be enhanced by incorporating hybrid modeling techniques, which combine machine learning and empirical correlations. These particular improvements will greatly increase the scientific contribution, robustness, and application of subsequent research in this area.

REFERENCES

[1] Kumar, R., Dubey, S., Sen, D., Mandal, S.K. (2024). A machine learning based approach for predicting pool boiling heat transfer coefficient of CNT + GO nanoparticle coated surfaces. International Communications in Heat and Mass Transfer, 154: 107455. https://doi.org/10.1016/j.icheatmasstransfer.2024.107455

[2] Gajghate, S.S., Baratula, S., Saha, B.B., Bhaumik, S. (2024). Maximizing heat transfer potential with graphene nanofluids along with structured copper surfaces for pool boiling. Thermal Science and Engineering Progress, 50: 102559. https://doi.org/10.1016/j.tsep.2024.102559

[3] Serrao, B.P., Kim, K.M., Duarte, J.P. (2023). Analysis of the effects of different nanofluids on critical heat flux using artificial intelligence. Energies, 16(12): 4762. https://doi.org/10.3390/en16124762

[4] Rashidi, M.M., Nazari, M.A., Harley, C., Momonia, E., Mahariq, I., Ali, N. (2022). Applications of machine learning methods for boiling modeling and prediction: A comprehensive review. Chemical Thermodynamics and Thermal Analysis, 8: 100081. https://doi.org/10.1016/j.ctta.2022.100081

[5] Fazel, S.A.A. (2024). Prediction of bubble departure diameter in pool boiling of mixtures by ANN using modified. ReLU. Heliyon, 10(11): e31261. https://doi.org/10.1016/j.heliyon.2024.e31261

[6] Mehdi, S., Nannapaneni, S., Hwang, G. (2022). Structural-material-operational performance relationship for pool boiling on enhanced surfaces using deep neural network model. 198: 123395. https://doi.org/10.1016/j.ijheatmasstransfer.2022.123395

[7] Rashidi, M.M., Alhuyi Nzari, M., Harley, C., Momoniat, E., Mahariq, I., Ali, N. (2022). Application of machine learning methods for boiling modelling and prediction: A comprehensive review. 8: 10081. https://doi.org/10.1016/j.ctta.2022.100081

[8] Hamzekhani, S., Shahraki, F., Mohebbi-Kalhori, D., Fardinpour, M.R. (2022). Experimental investigation and modeling of bubble departure frequency for nucleate pool boiling heat transfer of pure liquids on flat heater. International Journal of Advanced Design & Manufacturing Technology, 15(4): 71. https://doi.org/10.30486/admt.2023.1960198.1354

[9] Zhang, J.F., Zhong, D.W., Shi, H.P., Meng, J.A., Chen, L. (2022). Machine learning prediction of critical heat flux on downward facing surfaces. International Journal of Heat and Mass Transfer, 191: 122857. https://doi.org/10.1016/j.ijheatmasstransfer.2022.122857

[10] Rokoni, A., Zhang, L.G., Soori, T., Hu, H., Wu, T., Sun, Y. (2022). Learning new physical descriptors from reduced-order analysis of bubble dynamics in boiling heat transfer. International Journal of Heat and Mass Transfer, 186: 122501. https://doi.org/10.1016/j.ijheatmasstransfer.2021.122501

[11] Scariot, V.K., Hobold, G.M., da Silva, A.K. (2024). Data-driven diagnostics of boiling heat transfer on flat heaters from non-intrusive visualization. Applied Thermal Engineering, 248: 123068. https://doi.org/10.1016/j.applthermaleng.2024.123068

[12] McClure, E.R., Carey, V.P. (2021). Genetic algorithm and deep learning to explore parametric trends in nucleate boiling heat transfer data. Journal of Heat Transfer, 143(12): 121601. https://doi.org/10.1115/1.4052435

[13] Calati, M., Righetti, G., Doretti, L., Zilio, C., Longo, G.A., Hooman, K., Mancin, S. (2021). Water pool boiling in metal foams: From experimental results to a generalized model based on artificial neural network. International Journal of Heat and Mass Transfer, 176: 121451. https://doi.org/10.1016/j.ijheatmasstransfer.2021.121451

[14] Sajjad, U., Hussain, I., Wang, C.C. (2021). A high-fidelity approach to correlate the nucleate pool boiling data of roughened surfaces. International Journal of Multiphase Flow, 142: 103719. https://doi.org/10.1016/j.ijmultiphaseflow.2021.103719

[15] Peng, Y., Boroumand Ghahnaviyeh, M., Ahmad, M.N., Abdollahi, A., Bagherzadeh, S.A., Azimy, H., Mosavi, A., Karimipour, A. (2021). Analysis of the effect of roughness and concentration of Fe_3O_4/water nanofluid on the boiling heat transfer using the artificial neural network: An experimental and numerical study. International Journal of Thermal Sciences, 163: 106863. https://doi.org/10.1016/j.ijthermalsci.2021.106863

[16] Rassoulinejad-Mousavi, S.M., Al-Hindawi, F., Soori, T., Rokoni, A., Yoon, H., Hu, H., Wu, T., Sun, Y. (2021). Deep learning strategies for critical heat flux detection in pool boiling. Applied Thermal Engineering, 190: 116849. https://doi.org/10.1016/j.applthermaleng.2021.116849

[17] Sajjad, U., Hussain, I., Hamid, K., Bhat, S.A., Ali, H.M., Wang, C.C. (2021). A deep learning method for estimating the boiling heat transfer coefficient of porous surfaces. Journal of Thermal Analysis and Calorimetry, 145: 1913-1925. https://doi.org/10.1007/s10973-021-10606-8

[18] Pare, A., Ghosh, S.K. (2021). Surface qualitative analysis and ANN modelling for pool boiling heat transfer using Al_2O_3-water based nanofluids. Colloids and Surfaces A: Physicochemical and Engineering Aspects, 610: 125926. https://doi.org/10.1016/j.colsurfa.2020.125926

[19] Swain, S., Swain, A., Kar, S.P. (2021). Pool boiling heat transfer using isopropyl alcohol and ammonium chloride surfactant. In Proceedings of International Conference on Thermofluids. Lecture Notes in Mechanical Engineering, pp. 343-351. https://doi.org/10.1007/978-981-15-7831-

1_31
[20] Gajghate, S.S., Barathula, S., Das, S., Saha, B.B., Bhaumik, S. (2020). Experimental investigation and optimization of pool boiling heat transfer enhancement over graphene-coated copper surface. Journal of Thermal Analysis and Calorimetry, 140: 1393-1411. https://doi.org/10.1007/s10973-019-08740-5
[21] McClure, E.R., Carey, V.P. (2020). Use of genetic algorithms and machine learning to explore parametric trends in nucleate boiling heat transfer data. In Proceedings of the ASME 2020 Heat Transfer Summer Conference collocated with the ASME 2020 Fluids Engineering Division Summer Meeting and the ASME 2020 18th International Conference on Nanochannels, Microchannels, and Minichannels. https://doi.org/10.1115/HT2020-9077
[22] Zarei, M.J., Ansari, H.R., Keshavarz, P., Zerafat, M.M. (2020). Prediction of pool boiling heat transfer coefficient for various nano-refrigerants utilizing artificial neural networks. Journal of Thermal Analysis and Calorimetry, 139: 3757-3768. https://doi.org/10.1007/s10973-019-08746-z
[23] Alavi Fazel, S.A., Lorzadeh, E. (2020). Pool boiling heat transfer intensification by electro-stimulation. Chemical Engineering and Processing - Process Intensification, 149: 107818. https://doi.org/10.1016/j.cep.2020.107818
[24] Ravichandran, M., Bucci, M. (2019). Online, quasi-real-time analysis of high-resolution, infrared, boiling heat transfer investigations using artificial neural networks. Applied Thermal Engineering, 163: 114357. https://doi.org/10.1016/j.applthermaleng.2019.114357
[25] Mansour, T.M., Khalaf-Allah, R.A. (2020). Theoretical and experimental verification for determining pool boiling heat transfer coefficient using fuzzy logic. Heat and Mass Transfer, 56: 3059-3070. https://doi.org/10.1007/s00231-020-02917-7
[26] Qiu, Y., Vo, T., Garg, D., Lee, H., Kharangate, C.R. (2023). A systematic approach to optimization of ANN model parameters to predict flow boiling heat transfer coefficient in mini/micro-channel heatsinks. International Journal of Heat and Mass Transfer, 202: 123728. https://doi.org/10.1016/j.ijheatmasstransfer.2022.123728
[27] He, M., Lee, Y. (2019). Revisiting heater size sensitive pool boiling critical heat flux using neural network modeling: Heater length of the half of the Rayleigh-Taylor Instability Wavelength maximizes CHF. Thermal Science and Engineering Progress, 14: 100421. https://doi.org/10.1016/j.tsep.2019.100421
[28] Aliç, E., Daş, M., Kaska, O. (2019). Heat flux estimation at pool boiling processes with computational intelligence methods. Processes, 7(5): 293. https://doi.org/10.3390/pr7050293
[29] Gajghate, S., Acharya, A.R., Pise, A.T. (2014). Experimental study of aqueous ammonium chloride in pool boiling heat transfer. Experimental Heat Transfer, 27(2): 113-123. https://doi.org/10.1080/08916152.2012.757673
[30] Gajghate, S.S., Vashistha, S., Saha, B.B., Bhaumik, S. (2021). Experimental and numerical investigation of pool boiling heat transfer over different thickness of graphene–poly (3,4 Ethylene dioxythiophene): Poly (Styrenesulfonate) layers on copper heater surface. Heat Transfer Engineering, 42(13-14): 1203-1222. https://doi.org/10.1080/01457632.2020.1777013

NOMENCLATURE

ANN	artificial neural network
CHF	critical heat flux
BHTC	boiling heat transfer coefficient
LM	Levenberg Marquardt
SCG	Scaled Conjugate Gradient
MSE	mean square error
R^2	coefficient of correlation
RO	reverse osmosis
PBHTC	pool boiling heat transfer coefficient
CNT	carbon nano-tube
GO	graphene oxide
ReLU	rectified linear unit
ML	machine learning
AI	artificial intelligence
SVM	support vector machine

Subscripts

exp	experimental
pre	predicted